Control Strategy for Reduction of Current Distortion in Reverse Matrix Converter under Unbalanced Input Conditions

Dongho Choi and Yeongsu Bak
Department of Electrical and Computer Engineering
Ajou University
Suwon, South Korea
qjwjsqjwjs@ajou.ac.kr and wov2@ajou.ac.kr

Jong-Pil Lee and Tae-Jin Kim
Korea Electrotechnology Research Institute
Changwon, Korea
jplee@keri.re.kr and tjkim@keri.re.kr

Kyo-Beum Lee
Department of Electrical and Computer Engineering
Ajou University
Suwon, South Korea
kyl@ajou.ac.kr

***Abstract*—This paper proposes a control strategy for reduction of current distortion in reverse matrix converter (RMC) under unbalanced input conditions. In the distributed generation (DG) system, the RMC is used to transmit the power generated by renewable energy system (RES) to the grid. If the voltage of the RES has unbalanced conditions, the input and output currents of the RMC are distorted. The distortion of the output currents especially induces a ripple of power transmitted to the grid and it deteriorates the stability and reliability of the DG system. The proposed control strategy using positive and negative phase-sequence components of voltage and current reduces the distortion of both side currents of the RMC. The effectiveness of the proposed control strategy for reduction of current distortion is verified by simulation results.**

Keywords—Reverse Matrix Converter (RMC), unbalanced input condtions, current distortion, positive and negative phase-sequence components

I. INTRODUCTION

Recently, renewable energy system (RES) has become an important issue because of problems of environmental pollution, gradual depletion of energy resources, and global warming. The researches for the RES, which are wind power, bioenergy, and marine energy are actively progressed [1], [2]. The RES generates and supplies to power by connecting to the grid. However, the electricity using the RES is not able to sufficiently meet the electricity demands because the use of devices that consume electricity is increased. The electricity supply has become saturated because of environmental, social, and geographical factors. In order to overcome these problems and to meet the electrical energy demand, researches for microgrids and distributed generation (DG) system are progressed [3].

A centralized generation (CG) system is a method to supply electricity generated from large power plants using thermal, hydroelectric, and nuclear power. The electricity generated from the CG system is supplied to homes and building through the transmission and distribution network that is spread throughout the country. The DG system is a method to supply required electricity with electricity generation facilities in the building. In other words, it means a power generation system having distributed arrangement around demand area with a small scale contrary to fundamental CG system with a large scale. Since the DG system has less burden on the production of large capacity electricity than the CG system, it is advantageous to utilize the RES. In the DG system, it is not possible that the RES is directly connected to distribution grid because it has mismatches of the voltage magnitude and frequency. Generally, the voltage magnitude and frequency of the RES have variable value and those of the grid have fixed value. Therefore, the DG system are required to proper power convertors for connecting the RES to the grid. If the RES is

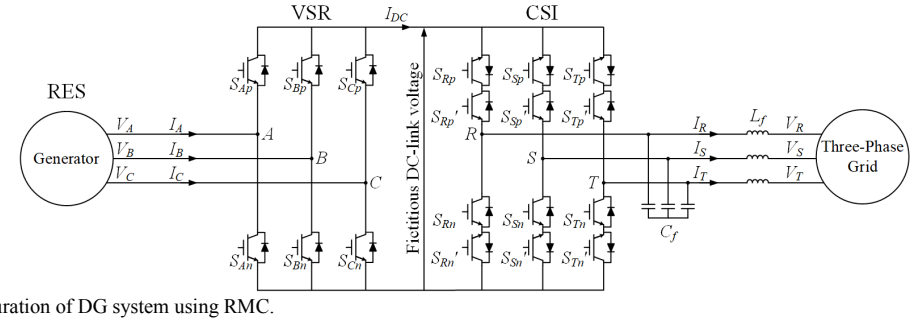

Fig. 1. Circuit configuration of DG system using RMC.

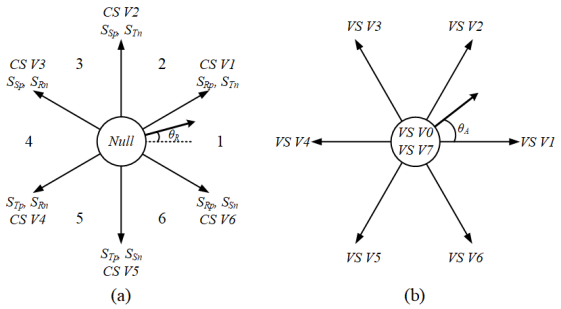

Fig. 2. Space vector diagrams of (a) CSI and (b) VSR.

composed of generators or turbines, AC/DC/AC or AC/AC power convertors are required.

One of the fundamental AC/DC/AC converters is a back-to-back (BTB) converter. The BTB converter has disadvantages such as short lifetime, large volume, and low durability because of bulky energy storage elements [4], [5]. In order to overcome the drawback of the BTB converter, researches for eliminating the energy storage elements of the DC-link are progressed. The indirect matrix converter (IMC) is one of the AC/AC converters without DC-link energy storage elements. It has structure similar to that of the BTB converter. The IMC has advantages such as small volume and high durability because it does not have DC-link energy storage elements [6], [7]. However, the IMC operates with an input-output maximum voltage transfer ratio of 0.866, which is critical drawback [8]. In other words, the IMC always operates in buck mode.

In the DG system, if the power generated by the RES have smaller magnitude voltage than that of the grid, the power converters operating in the boost mode are required in order to transmit the power to grid. The IMC operating in buck mode cannot be used to transmit the power. In order to maintain advantages of the IMC due to absence of the DC-link energy storage elements and to have application in the DG system, the topology and control strategy of the IMC operating in boost mode have been researched [9]. It is called a reverse matrix converter (RMC) because the power direction of the IMC is reversed in order to improve the voltage transfer ratio of the IMC. The RMC that reverses the input to the output in the IMC has a minimum voltage transfer ratio over 1/0.866. The RMC is composed of a voltage source rectifier (VSR) and current source inverter (CSI). Therefore, in the DG system using the RMC, the VSR and CSI of the RMC are connected by the RES and the grid, respectively.

The power generated by the RES having low voltage magnitude is directly transmitted by the RMC to the grid without DC-link energy storage elements. If the RES generates the three-phase voltage under unbalanced conditions, the currents of the VSR and CSI stage, which are input and output stage of the RMC, are distorted [10]. The distorted currents have a bad influence on the grid. This paper proposes a control strategy for reduction of the current distortion under unbalanced conditions of the RES, which are connected by the VSR stage of the RMC for the DG system. The effectiveness of the proposed control strategy is verified by simulation results.

II. CIRCUIT CONFIGURATION AND MODULATION STRATEGY

A. Circuit Configuration

Fig. 1 shows overall circuit configuration of the DG system using the RMC. The RMC is composed of VSR and CSI through the fictitious DC-link. Each of VSR and CSI respectively consist of 6- and 12-bidirectional switches. The input stage of the RMC is connected with generator based on RES. The output stage of the RMC is connected with three-phase grid through filter inductors and capacitors which reduce the current and voltage ripple of overall systems. The power generated from the RES is transmitted to the three-phase grid through the RMC.

B. Modulation Strategy of the CSI

The space vector diagram of the CSI is shown in Fig. 2(a). There are six active states and three null states. In the active states, the fictitious DC-link voltage is produced by synthesized two line-to-line voltages which are maximum and second largest magnitudes of the three-phase grid. In this case, the power generated from the RES is transmitted to the three-phase grid across the fictitious DC-link. In the null states, the fictitious DC-link voltage is shorted to zero.

A reference current phasor is reproduced using the nearest two vectors in Fig. 2(a). If a reference current phasor belongs to sector 1, it is formed using *CS V1* and *CS V6*. In this instance, the upper switch of *R*-phase leg (S_{Rp}) is turned ON during the full switching time, with the result that the upper DC-link is clamped with *R*-phase voltage of the three-phase grid. In contrast, the two lower switches (S_{Sn}, S_{Tn}) are modulated using active duty ratios (d_x, d_y) and thus the lower DC-link is clamped with *S*-phase and *T*-phase alternately depending on the switching state of the lower switches. The active duty ratios for modulation of the CSI are derived as follows. First of all, each reference phase current of the CSI stage is represented as in (1).

$$I_R^* = I_{om}\cos\theta_R,\ I_S^* = I_{om}\cos\theta_S,\ I_T^* = I_{om}\cos\theta_T,\\ \left(\theta_R = \omega_o t,\ \theta_S = \theta_R - 2\pi/3,\ \theta_T = \theta_R - 4\pi/3\right) \tag{1}$$

where I_{om} is current amplitude and θ_R, θ_S and θ_T are respective phase angles. Secondly, since the sum of three-phase currents are zero, the active duty ratios (d_x, d_y) are calculated as in (2).

$$\cos\theta_R + \cos\theta_S + \cos\theta_T = 0,\quad -\frac{\cos\theta_S}{\cos\theta_R} - \frac{\cos\theta_T}{\cos\theta_R} = 1,\\ d_x = -\frac{\cos\theta_S}{\cos\theta_R},\quad d_y = -\frac{\cos\theta_T}{\cos\theta_R}. \tag{2}$$

Furthermore, an average fictitious DC-link voltage is calculated by multiplying the duty ratios and line-to-line voltages (V_{RS}, V_{RT}) of the three-phase grid. It is expressed as in (3).

$$V_{DC(av)} = d_x V_{RS} + d_y V_{RT} = 1.5\cdot\left(V_{om}/\cos\theta_R\right)\cdot\cos\phi_o,\\ \left(-\pi/6 \le \theta_R \le \pi/6\right) \tag{3}$$

where V_{om} is phase voltage amplitude and ϕ_o is output power factor. The same interpretation can be applied to the reference current phasor in other five sectors.

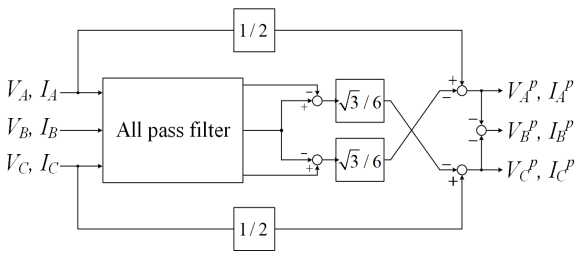

(a)

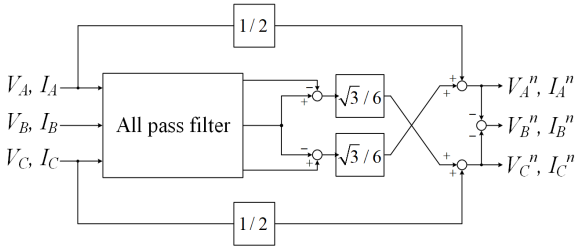

(b)

Fig. 3. Detection block diagrams of (a) positive and (b) negative phase-sequence components.

C. Modulation Strategy of the VSR

The modulation strategy of the VSR is similar to the common two-level inverter. The space vector diagram of the VSR is shown in Fig. 2(b). Depending on the switching states, the space vectors are divided into two classes, which are six active states and two null states. The null states, meaning the zero vectors such as *VS V0* and *VS V7*, occur by turning ON either all upper (S_{Ap}, S_{Bp}, S_{Cp}) or lower switches (S_{An}, S_{Bn}, S_{Cn}) of the VSR. The modulation of the VSR is performed by the carrier based method after the $V_{DC(av)}$ is compensated to produce sinusoidal input and output currents. The two modulation signals ($V_{j(upper)}$, $V_{j(lower)}$ | $j = A, B, C$) of each phase are indicated as in (4).

$$
\begin{aligned}
&V_{j(upper)|j=A,B,C} = -2d_y \cdot \frac{V_j^* + V_{off}}{V_{DC(av)}} + d_x, \\
&V_{j(lower)|j=A,B,C} = 2d_x \cdot \frac{V_j^* + V_{off}}{V_{DC(av)}} - d_y, \\
&\left(V_{off} = -\left[\max(V_A^*, V_B^*, V_C^*) + \min(V_A^*, V_B^*, V_C^*)\right]/2\right).
\end{aligned} \tag{4}
$$

where V_j^* ($j = A, B, C$) is reference voltage of the each phase and V_{off} is offset voltage of the three-phase reference voltages. Switching operation of the VSR is implemented by comparing the two modulations with triangular carrier.

III. Proposed Control Strategy for Reduction of Current Distortion

A. Detection Method of Positive and Negative Phase-Sequence Components

In the DG system using the RMC, input and output currents of the RMC under unbalanced input conditions are distorted. The distortion of the output currents especially deteriorates the stability and reliability of the DG system. Therefore, a control strategy for reduction of the output currents distortion is required. This paper presents a control strategy using positive and negative phase-sequence components in order to reduce the output currents distortion.

The unbalanced voltages are composed of positive and negative phase-sequence components. In addition, distorted currents due to unbalanced input conditions contain negative phase-sequence components. In this paper, each component of the currents is controlled using the proposed control strategy to reduce the current distortion. Since the proposed control strategy requires to positive and negative phase-sequence components of voltages and currents under unbalanced input conditions, detections for the components are progressed before applying the proposed control strategy.

In terms of input voltages of the RMC, the positive (V_A^p, V_B^p, V_C^p) and negative phase-sequence components (V_A^n, V_B^n, V_C^n) under unbalanced voltage conditions are obtained using symmetrical coordinates method as shown in Fig. 3. Regarding input currents, identical method can be applied.

B. Calculation of New Reference Currents

The complex power generated from the RES has AC components due to distorted currents containing negative phase-sequence components under unbalanced voltage conditions. In order to eliminate those AC components, in this paper, the new reference currents are calculated. This process leads to balanced complex power result in reduced current distortion. The complex power of the input stage is represented in the *d-q* axis synchronous frame as in (5).

$$
\begin{aligned}
&S = \frac{3}{2}(V_{dq}^p e^{j\omega t} + V_{dq}^n e^{-j\omega t})\overline{(I_{dq}^p e^{j\omega t} + I_{dq}^n e^{-j\omega t})}, \\
&V_{dq}^p = V_d^p + jV_q^p, \quad V_{dq}^n = V_d^n + jV_q^n, \\
&I_{dq}^p = I_d^p + jI_q^p, \quad I_{dq}^n = I_d^n + jI_q^n,
\end{aligned} \tag{5}
$$

where V_{dq}^p, V_{dq}^n, I_{dq}^p, and I_{dq}^n are positive and negative phase-sequence components of voltages and currents in the *d-q* axis synchronous frame. The complex power is composed of active power and reactive power as in (6).

$$
\begin{aligned}
&P(t) = P_0 + P_{\cos 2}\cos(2\omega t) + P_{\sin 2}\sin(2\omega t), \\
&Q(t) = Q_0 + Q_{\cos 2}\cos(2\omega t) + Q_{\sin 2}\sin(2\omega t).
\end{aligned} \tag{6}
$$

The active and reactive power consist of DC components such as P_0, Q_0 and AC components such as P_{cos2}, P_{sin2}, Q_{cos2}, and Q_{sin2} vibrating to two times of the generator frequency. The DC and AC components excluding of Q_{cos2} and Q_{sin2} are represented using V_{dq}^p, V_{dq}^n, I_{dq}^p, and I_{dq}^n as in (7).

$$
\begin{aligned}
&P_0 = (3/2)\left(V_d^p I_d^p + V_q^p I_q^p + V_d^n I_d^n + V_q^n I_q^n\right), \\
&Q_0 = (3/2)\left(V_q^p I_d^p - V_d^p I_q^p + V_q^n I_d^n + V_d^n I_q^n\right), \\
&P_{\cos 2} = (3/2)\left(V_d^n I_d^p + V_q^n I_q^p + V_d^p I_d^n + V_q^p I_q^n\right), \\
&P_{\sin 2} = (3/2)\left(V_q^n I_d^p - V_d^n I_q^p - V_q^n I_d^n + V_d^p I_q^n\right).
\end{aligned} \tag{7}
$$

In (7), P_{cos2} and P_{sin2} are substitute to zero for eliminating AC components of active power. P_0 and Q_0 are indicated by input active and reactive power (P_{in}, Q_{in}), respectively. The new reference currents are determined as in (8).

$$
\begin{aligned}
&I_d^{p*} = \frac{2V_d^p}{3X}P_{in}^* + \frac{2V_q^p}{3Y}Q_{in}^*,\ I_q^{p*} = \frac{2V_q^p}{3X}P_{in}^* - \frac{2V_d^p}{3Y}Q_{in}^*,\\
&I_d^{n*} = -\frac{2V_d^n}{3X}P_{in}^* + \frac{2V_q^n}{3Y}Q_{in}^*,\ I_q^{n*} = -\frac{2V_q^n}{3X}P_{in}^* - \frac{2V_d^n}{3Y}Q_{in}^*, \quad (8)\\
&\begin{pmatrix} X = \left[(V_d^p)^2 + (V_q^p)^2\right] - \left[(V_d^n)^2 + (V_q^n)^2\right], \\ Y = \left[(V_d^p)^2 + (V_q^p)^2\right] + \left[(V_d^n)^2 + (V_q^n)^2\right] \end{pmatrix}.
\end{aligned}
$$

Each input active and reactive reference power, under balanced voltage conditions, can be represented with reference currents as in (9).

$$
P_{in}^* = \frac{3X}{2V_q^p}I_{qe}^*,\quad Q_{in}^* = \frac{3Y}{2V_q^p}I_{de}^* \tag{9}
$$

By substituting (9) into (8), positive and negative phase-sequence components of the new reference currents for reduction of the current distortion can be obtained as in (10).

$$
\begin{aligned}
&I_d^{p*} = \frac{V_d^p}{V_q^p}I_{qe}^* + I_{de}^*,\quad I_q^{p*} = I_{qe}^* - \frac{V_d^p}{V_q^p}I_{de}^*,\\
&I_d^{n*} = -\frac{V_d^n}{V_q^p}I_{qe}^* + \frac{V_q^n}{V_q^p}I_{de}^*,\quad I_q^{n*} = -\frac{V_q^n}{V_q^p}I_{qe}^* - \frac{V_d^n}{V_q^p}I_{de}^*
\end{aligned} \tag{10}
$$

C. Control Block Diagram of the RMC under Unbalanced Input Conditions

A control block diagram of the RMC in the DG system under unbalanced input conditions is shown in Fig. 4. In the CSI stage, three-phase currents (I_R, I_S, I_T) are transformed to *d-q* axis synchronous frame using phase angle (θ_g) of the three-phase grid. The *d-q* axis synchronous frame currents of the CSI stage (I_{de_out}, I_{qe_out}) are controlled to reference current ($I^*_{de\_out}$, $I^*_{qe\_out}$) using proportional-integral (PI) controller. After that, the switching operation is performed by the modulation method with (1) to (3). In the VSR stage, three-phase currents (I_A, I_B, I_C) are controlled using the proposed control strategy.

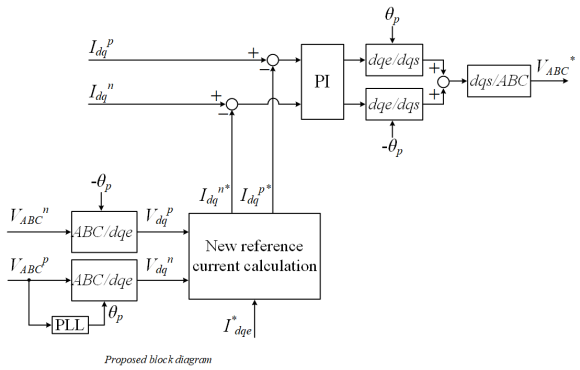

Fig. 5. Control block diagram of the proposed control strategy.

The control block diagram of the proposed control strategy is shown in Fig. 5. The detection of positive and negative phase-sequence components of the voltages and currents is implemented in the Fig 3. The new reference currents (I_{dq}^{p*}, I_{dq}^{n*}) are calculated with (10) under unbalanced input conditions. As a result, the positive and negative phase-sequence components of the currents (I_{dq}^{p}, I_{dq}^{n}) are controlled to the new reference currents using PI controllers, respectively. The controller outputs (V_{ABC}^*) are modulated with (4) and the switching operation is carried out by the carrier based PWM.

D. Control Algorithm for Reduction of Harmonics

A control algorithm for reduction of harmonics in the input currents is required to improve the quality of power transmitted to the three-phase grid from the RES. In the DG system using the RMC, if harmonics are contained in the input currents of the RMC, those are indicated in the output currents as well. The harmonics of the output currents aggravate the quality of three-phase grid. Particularly, since the 5th and 7th order harmonics in the input currents are dominant, they must be dealt with properly. The *d-q* axis synchronous frame input currents (I_{de}, I_{qe}) containing the harmonics can be expressed by Fourier transform as in (11). The 5th and 7th order harmonics in the stationary frame are represented as 6th order harmonics in the synchronous frame.

$$
\begin{aligned}
I_{de} &= I_{om}\left\{(1/5)\cdot\sin(6\omega t) + (1/7)\cdot\sin(6\omega t) + \cdots\right\},\\
I_{qe} &= I_{om}\left\{-1 + (1/5)\cdot\cos(6\omega t) - (1/7)\cdot\cos(6\omega t) + \cdots\right\}
\end{aligned} \tag{11}
$$

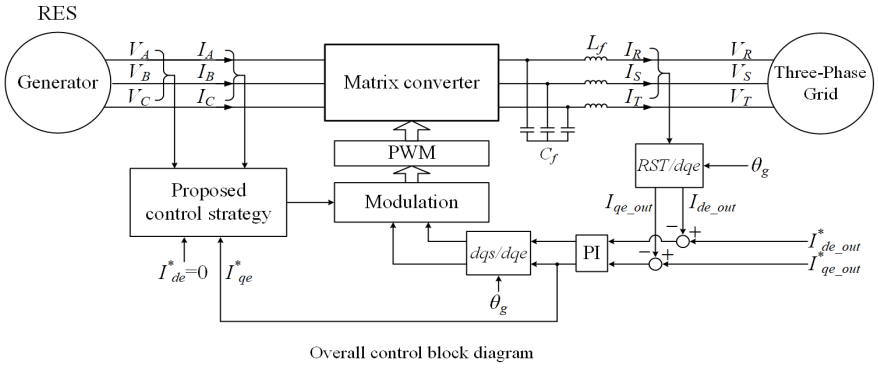

Fig. 4. Control block diagram of the RMC in DG system under unbalanced input conditions.

TABLE I. SIMULATION PARAMETERS

Variables	Value
Generator line-to-line voltage	150 V_{rms}
Generator frequency	30 Hz
Grid line-to-line voltage	380 V_{rms}
Grid frequency	60 Hz
Control period	100 μs

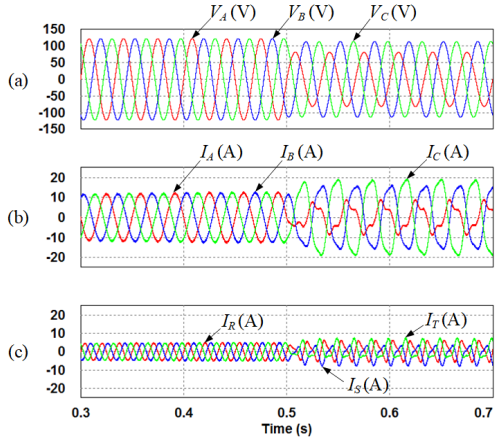

Fig. 6. Simulation results of current control under unbalanced input conditions without proposed control strategy.

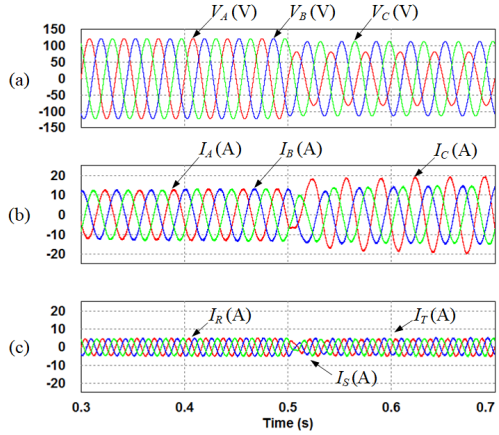

Fig. 7. Simulation results of current control under unbalanced input conditions with proposed control strategy.

The 5th and 7th order harmonics in the input currents can be reduced through the control of 6th order harmonics in the synchronous frame to zero, with the result that quality of the output currents can be improved.

IV. SIMULATION RESULTS

The proposed control strategy was simulated using PSIM software and the simulation parameters are described in Table I. Fig. 6 and Fig. 7 show simulation results of current control under unbalanced input conditions. Figs. 6(a) and (b) show input phase voltages and currents and Fig. 6(c) shows output phase currents. Fig. 7 has a scenario similar to that of the Fig. 6.

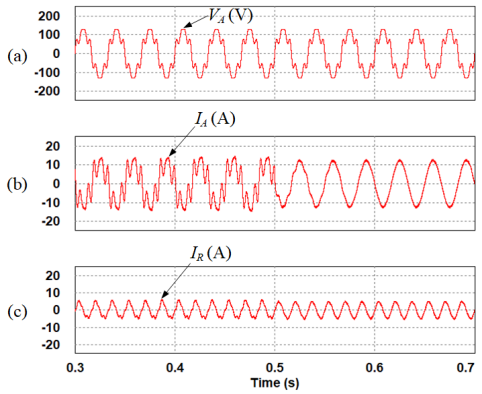

Fig. 8. Simulation results of control algorithm for reduction of harmonics under balanced input conditions (a) Input *A*-phase voltage. (b) Input *A*-phase current. (c) Output *R*-phase current.

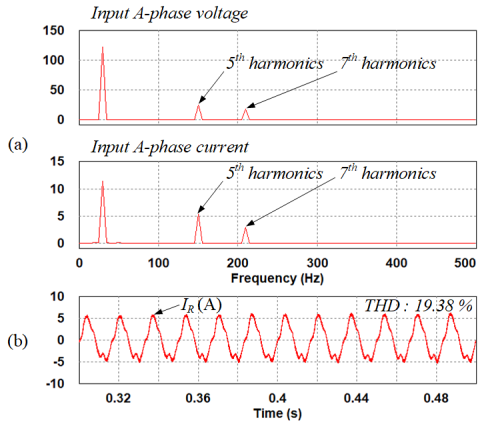

Fig. 9. (a) FFT analysis of the input *A*-phase voltage and current without control algorithm for reduction of harmonics (b) Output *R*-phase current.

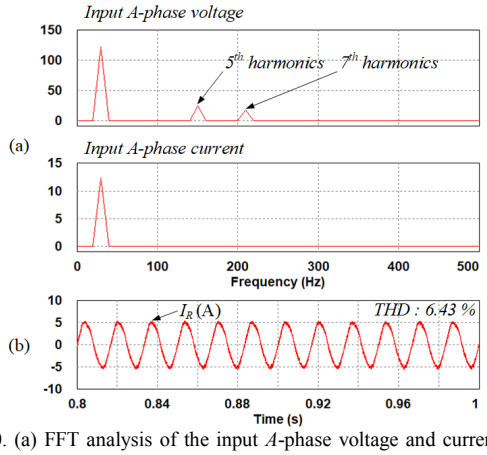

Fig. 10. (a) FFT analysis of the input *A*-phase voltage and current with control algorithm for reduction of harmonics (b) Output *R*-phase current.

However, in the Fig. 7, the proposed control strategy is applied for reduction of the current distortion contrary to the Fig. 6. In these simulation results, *d*-axis and *q*-axis current are controlled 0 A and 5 A, respectively. From 0.5 s, the amplitude of the *A*-phase voltage is decreased to 75 V_{rms}. In Fig. 6, under unbalanced input conditions, input and output currents are distorted. Contrary to Fig. 6, in Fig.7, the input and output current distortion under unbalanced input conditions are reduced by the proposed control strategy.

In addition, the control algorithm for reduction of harmonics was also simulated under balanced input conditions as shown in Fig. 8. In case input *A*-phase current contains 5th and 7th order harmonics, the output *R*-phase current is a non-sinusoidal waveform because of the harmonics. The control algorithm for reduction of harmonics is applied from 0.5 s and the input and output currents are appeared as sinusoidal waveform. Fig. 9(a) and Fig. 10(a) show FFT analysis of the input *A*-phase voltage and current depending on the control algorithm for reduction of harmonics. The 5th and 7th order harmonics of the input *A*-phase current are reduced as shown in Fig. 10(a) compared with the harmonics as shown in Fig. 9(a). Fig. 9(b) and Fig. 10(b) show the output *R*-phase current. The THD of the output *R*-phase current is reduced from 19.38 % to 6.43 %.

V. CONCLUSIONS

In case the unbalanced voltage occurs in DG system using the RMC, the input and output currents are distorted. As proposed in this paper, the reduction of current distortion is achieved under unbalanced input conditions. Since the output current distortion is reduced using the proposed control strategy, the output power transmitted to the grid is in balanced conditions. Therefore, the stability and reliability of DG system using RMC is improved in that the balanced power is transmitted to the grid. Furthermore, additional control algorithm for reduction of harmonics is also introduced to enhance the quality of the output currents transmitted to the grid. The simulation results have demonstrated the validity of the proposed control strategy.

REFERENCES

[1] K. V. Iyer, R. Baranwal, and N. Mohan "A High-Frequency AC-Link Single-Stage Asymmetrical Multilevel Converter for Grid Integration of Renewable Energy Systems," *IEEE Trans. Power Electron.*, vol. 32, no. 7, pp. 5087–5108, Jul. 2017.

[2] M. Pahlevani, S. Eren, J. M. Guerrero, and P. Jain, "A Hybrid Estimator for Active/Reactive Power Control of Single-Phase Distributed Generation Systems With Energy Storage," *IEEE Trans. Power Electron.*, vol. 31, no. 4, pp. 2919–2936, Apr. 2016.

[3] F. Nejabatkhah, Y. Wei, and B. Wu, "Control Strategies of Three-Phase Distributed Generation Inverters for Grid Unbalanced Voltage Compensation," *IEEE Trans. Power Electron.*, vol. 31, no. 7, pp. 5228–5241, Jul. 2016.

[4] T. Friedli, J. W. Kolar, J. Rodriguez, and P. W. Wheeler, "Comparative Evaluation of Three-Phase AC-AC Matrix Converter and Voltage DC-Link Back-to-Back Converter Systems," *IEEE Trans. Ind. Electron.*, vol. 59, no. 12, pp. 4487–4510, Dec. 2012.

[5] J.-S. Lee, K.-B. Lee, and F. Blaabjerg, "Open-Switch Fault Detection Method of a Back-to-Back Converter Using NPC Topology for Wind Turbine Systems," *IEEE Trans. Ind. Appl.*, vol. 51, no. 1, pp. 325–335, Jan./Feb. 2015.

[6] Y. Bak, E. Lee, and K.-B. Lee, "Indirect Matrix Converter for Hybrid Electric Vehicle Application with Three-Phase and Single-Phase Outputs," *Energies*, vol. 8, no. 5, pp. 3849–3866, Apr. 2015.

[7] Y. Bak and K.-B. Lee, "Discontinuous PWM for Low Switching Losses in Indirect Matrix Converter Drives," *in Proc. APEC Conf.*, 2016, pp. 2764–2769.

[8] E. Lee and K.-B. Lee, "Fault Diagnosis for a Sparse Matrix Converter using Current Patters," *in Proc. APEC Conf.*, 2012, pp. 1549–1554.

[9] X. Liu, P. C. Loh, P. Wang, F. Blaabjerg, Y. Tang, and E. A. Al-Ammar, "Distributed Generation Using Indirect Matrix Converter in Reverse Power Mode," *IEEE Trans. Power Electron.*, vol. 28, no. 3, pp. 1072–1082, Mar. 2013.

[10] K. Park, K.-B. Lee, and F. Blaabjerg, "Improving Output Performance of a Z-Source Sparse Matrix Converter Under Unbalanced Input-Voltage Conditions," *IEEE Trans. Power Electron.*, vol. 27, no. 4, pp. 2043–2054, Apr. 2012.